Electronic supplementary information

Electrothermal based active control of ion transport in microfluidic device with ion-permselective membrane

Sinwook Park and Gilad Yossifon*

Faculty of Mechanical Engineering, Micro- and Nanofluidics Laboratory, Technion – Israel Institute of Technology, Technion City 3200000, Israel

1. Movies

Movie 1: Time evolution of the depletion layer at the anodic side of the microchannel-membrane interface ($d = 100\mu$m), with various heating powers: (1) no heating; (2) 16 mW; (3) 64 mW; (4) 100 mW. The heater was initially activated with application of a step-wise current of 75nA.

Movie 2: Time evolution of the depletion layer at the anodic side of the microchannel-membrane interface ($d = 330\mu$m) with various heating powers: (1) no heating; (2) 16 mW; (3) 60 mW; (4) 90 mW. The heater was initially activated with application of a step-wise current of 375nA.

Movie 3: Time evolution of the depletion layer at the anodic side of the microchannel-membrane interface ($d = 1000\mu$m) with various heating power: (1) no heating; (2) 16 mW; (3) 36 mW; (4) 60 mW. The heater was initially activated with application of a step-wise current of 720nA.

Movie 4: Time evolution of dynamic control of CP by the periodic step-wise application of the heater (60 mW), with a constant current (720 nA) within the microchannel ($d = 1000\mu$m).

2. Numerical Simulations

Here we solved the combined ET, natural convection and electro-osmosis effects on the depletion layer dynamics, via the fully coupled, two-dimensional (2D), time-dependent model using the finite-element based software COMSOL (V5.3). The simplifying assumptions used are symmetric and binary electrolyte ($z_+ = -z_- = 1$) and an ideal-permselective membrane. The governing equations in the system are the continuity of ions, $c_\pm$, using the Nernst−Planck relation for the ion fluxes, $\mathbf{j}_\pm$, including the convective term

$$\frac{\partial c_\pm}{\partial t} = -\nabla \cdot \mathbf{j}_\pm, \quad \mathbf{j}_\pm = -D_\pm \nabla c_\pm \mp \frac{F}{RT} D_\pm c_\pm \nabla \phi + \mathbf{u} c_\pm, \tag{3}$$

the Poisson equation for the electric potential, ϕ, in terms of the excess ionic charge density, ρ_e

$$\nabla^2 \phi = -\rho_e / \varepsilon; \quad \rho_e = F \sum_i z_i c_i, \tag{4}$$

the incompressible Navier-Stokes equations with both electrothermal (eq.(1)) and natural convection forcing using the Boussinesq approximation

$$\rho \frac{\partial \mathbf{u}}{\partial t} = -\nabla p + \eta \nabla^2 \mathbf{u} + \mathbf{f}_{\mathrm{ET}} + \rho \beta_T \mathbf{g} \Delta \mathrm{T}, \quad \nabla \cdot \mathbf{u} = 0, \tag{5}$$

and the energy equation for calculation of the temperature field, *T*, including the Joule heating, $\phi_{\&}$, effect[1]

$$\rho c_p \left(\partial T / \partial t + \left(\mathbf{u} \cdot \nabla T \right) \right) = k_f \nabla^2 T + \phi_{\&}. \tag{6}$$

Herein, , *F* is the Faraday constant, *R* is the universal gas constant, *T* is the temperature, *p* is the pressure, β_T is the fluid thermal expansion coefficient, *g* is the gravitational acceleration, ρ is the fluid mass density at room temperature, c_p is the fluid specific heat capacity and k_f is the fluid thermal conductivity. Here, temperature-dependent physical properties[2] were considered for ε_r, *D*, η and k_f: $\varepsilon_r = \varepsilon_{r,ref}(1 - 1.2984(T - T_{ref})/T_{ref})$, $D_+ = D_{+,ref}(1 + 8.4585(T - T_{ref})/T_{ref})$, $D_- = D_{-,ref}(1 + 8.8466(T - T_{ref})/T_{ref})$, $\eta = \eta_{ref} \exp(-6.46(T - T_{ref})/T_{ref})$ and $k_f = k_{f,ref}(1 + 0.8098(T - T_{ref})/T_{ref})$ where the reference values at $T_{ref} = 293K$ of $\varepsilon_{r,ref} = 80$, $D_{+,ref} = 1.96 \cdot 10^{-9} m^2 s^{-1}$, $D_{-,ref} = 2.03 \cdot 10^{-9} m^2 s^{-1}$, $\eta_{ref} = 0.001 kgm^{-3}$ and $k_{f,ref} = 0.6$. A prefactor of 3 was used for the ET force in eq.(5) for better fitting of the experimental results.

In our system the contribution of the Joule heating resulting from application of the external electric field at the reservoirs driving the CP, is much smaller (power applied on the external electrodes < 12μW) than that of the heater (32-90mW), hence, it can be neglected. In addition, the thermal Peclet number $\mathrm{Pe}_T = \rho c_p u d / k_f < 0.26$ for $u < 50\,\mu m s^{-1}$ is small, hence, the thermal convective term can be neglected, thus, suggesting decoupling of the thermal and electrokinetic problems. Estimation of the thermal relaxation time ($t_{diff} \approx 0.76\,\mathrm{s}$) from Wood et al.[2] suggests that the thermal problem can be treated as steady-state. Hence, Eq.(6) can be simplified to

$$k_f \nabla^2 T = 0\,. \tag{7}$$

The numerical 2D model consisted of a microchannel (length L=5mm, height d=0.75mm), with embedded heaters interfacing the anodic side of an ideal cation-permselective membrane (height d_n=200nm) (Fig. S1). The boundary conditions at the membrane interface ($x = 0, y \in [0, h_n]$) were no penetration of anions ($j_- = 0$), fixed cation concentration ($c_+ = N c_0$), and Donnan potential ($-RT/F \cdot \ln(N)$), with values $c_0 = 1 \cdot 10^{-3}\,\mathrm{mol\,m^{-3}}$ and $N = 10$. At the reservoir boundary ($x = L, y \in [0, h_m]$), a constant bulk concentration ($c_+ \approx c_- \equiv c_0$) is imposed along with uniform current density in terms of the electric displacement ($\mathrm{D}_{\mathrm{elec}} = -\varepsilon(RT/F)(1/2FDc_0)\mathrm{i}$). An overlimiting current density ($i = 1.45 i_{lim,1D}$, $i_{lim,1D} = 2\mathrm{D}Fc_0 / L$) was applied. At the other channel walls, no-penetration conditions and electrical insulation were used. For the electro-convective problem, the Helmholtz-Smoluchowski (HS) silp velocity, $u = -\varepsilon\zeta E_t / \eta$ (wherein ζ = -10 mV is the zeta potential and E_t is the tangential electric field component) was used at the channel walls and open boundary condition at the reservoir.

The heater has a serpentine geometry with an electrode width of 25μm, with its outer edges located at 500μm and 725μm from the membrane. For the thermal problem, a uniform heat flux ($q_0'' = P_r / A_{heater}$ where P_r and A_{heater} are the resistive heating power and area of heater) was used at the heater surface and constant room temperature (T_0 = 293.5 K) at the reservoir. Instead of also solving for the PDMS and glass domains, these were accounted for by including their thermal resistances as boundary conditions

$$(T - T_\infty) / R_s = -k_f \nabla T\,, \tag{8}$$

where for the PDMS upper layer the thermal resistance (per unit area), $R_{s,PDMS1} = t_{PDMS} / k_{PDMS} + 1/h$, consists of both conduction and convection contributions in series[1] with thickness $t_{PDMS1} = 3\,\text{mm}$, thermal conductivity $k_{PDMS} = 0.27\,\text{Wm}^{-1}\text{K}^{-1}$ and natural convection heat-transfer coefficient of $h \approx 10\text{Wm}^{-2}\text{K}^{-1}$. At the lower surface interfacing a glass of thickness $t_{\text{glass}} = 1\,\text{mm}$ and thermal conductivity $k_{\text{glass}} = 1.3\ \text{Wm}^{-1}\text{K}^{-1}$, and at the PDMS side wall with thickness $t_{PDMS2} = 1\,\text{mm}$, only the thermal resistances (per unit area) due to conduction are accounted for, i.e. $R_{s,\text{glass}} = t_{\text{glass}} / k_{\text{glass}}$ and $R_{s,PDMS2} = t_{PDMS2} / k_{PDMS}$, respectively, since isothermal conditions are assumed at the glass and the PDMS outer surfaces, due to its direct contact with the microscope stage and the solution in a cathode channel.

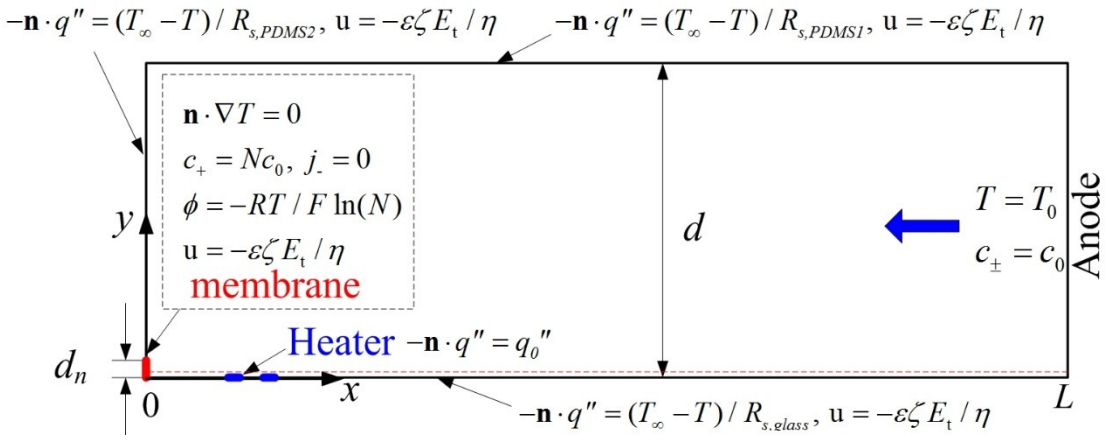

Supplementary Figure 1: Schematics of the 2D geometry and boundary conditions used in the numerical simulation for the microchannel domain at the anodic side of the membrane.

Reference

1 M. Zehavi, A. Boymelgreen and G. Yossifon, *Phys. Rev. Appl.*, 2016, **5**, 044013.

2 J. A. Wood, A. M. Benneker and R. G. H. Lammertink, *J. Phys. Condens. Matter*, 2016, **28**, 114002.

3. Supporting figures

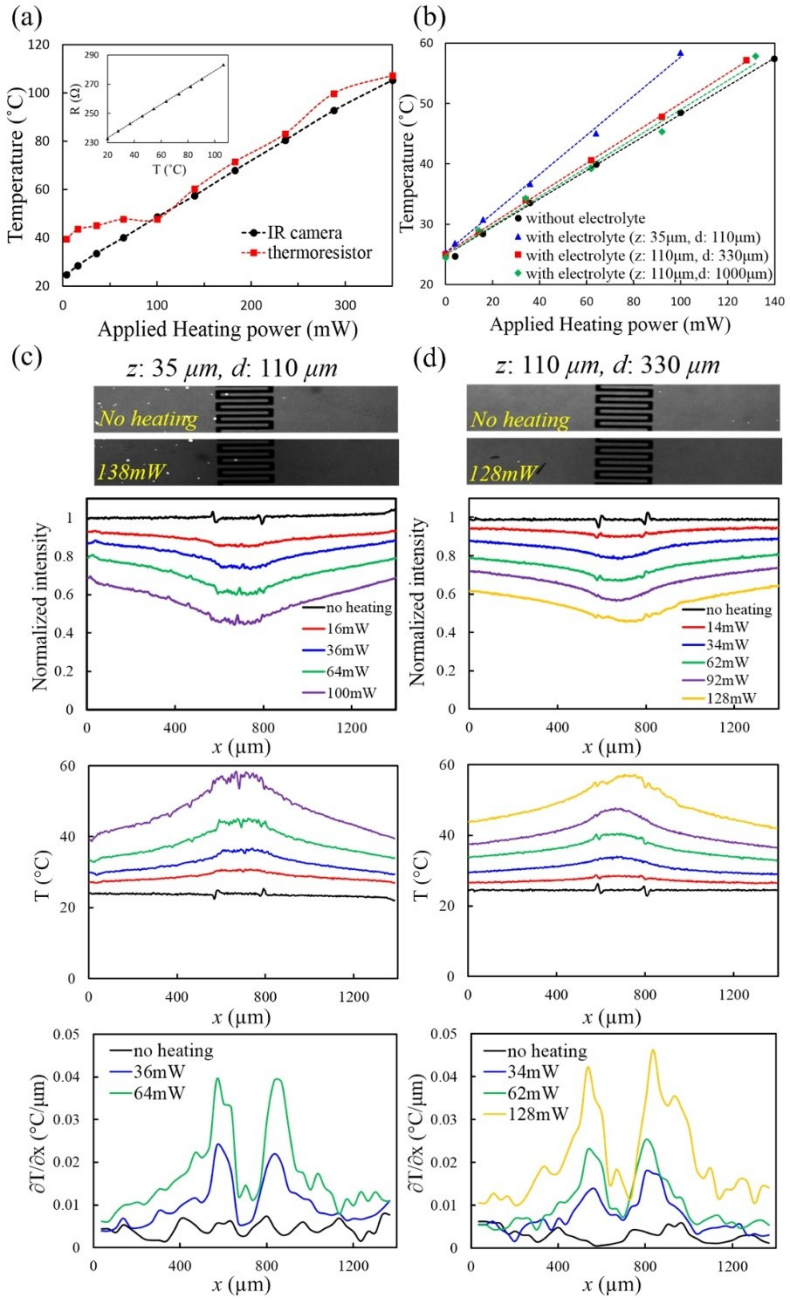

Supplementary Figure 2: (a) The heater temperature dependency on the heater power, as determined via IR camera and thermoresistor effect (without electrolyte). Inset indicates a linear relationship between the resistance of the heater and its temperature, from which the coefficient of resistance $\alpha = 0.0025$ is obtained. (b) The maximum temperature dependency on the heater power, as determined using rhodamine B fluorescent dye (with electrolyte) in microchannels with various depths. (c, d) Microscopic images and normalized intensity of rhodamine B fluorescent dye in the microchannels at t = 400s, for varying heater powers, and their corresponding temperature fields and temperature gradient fields.

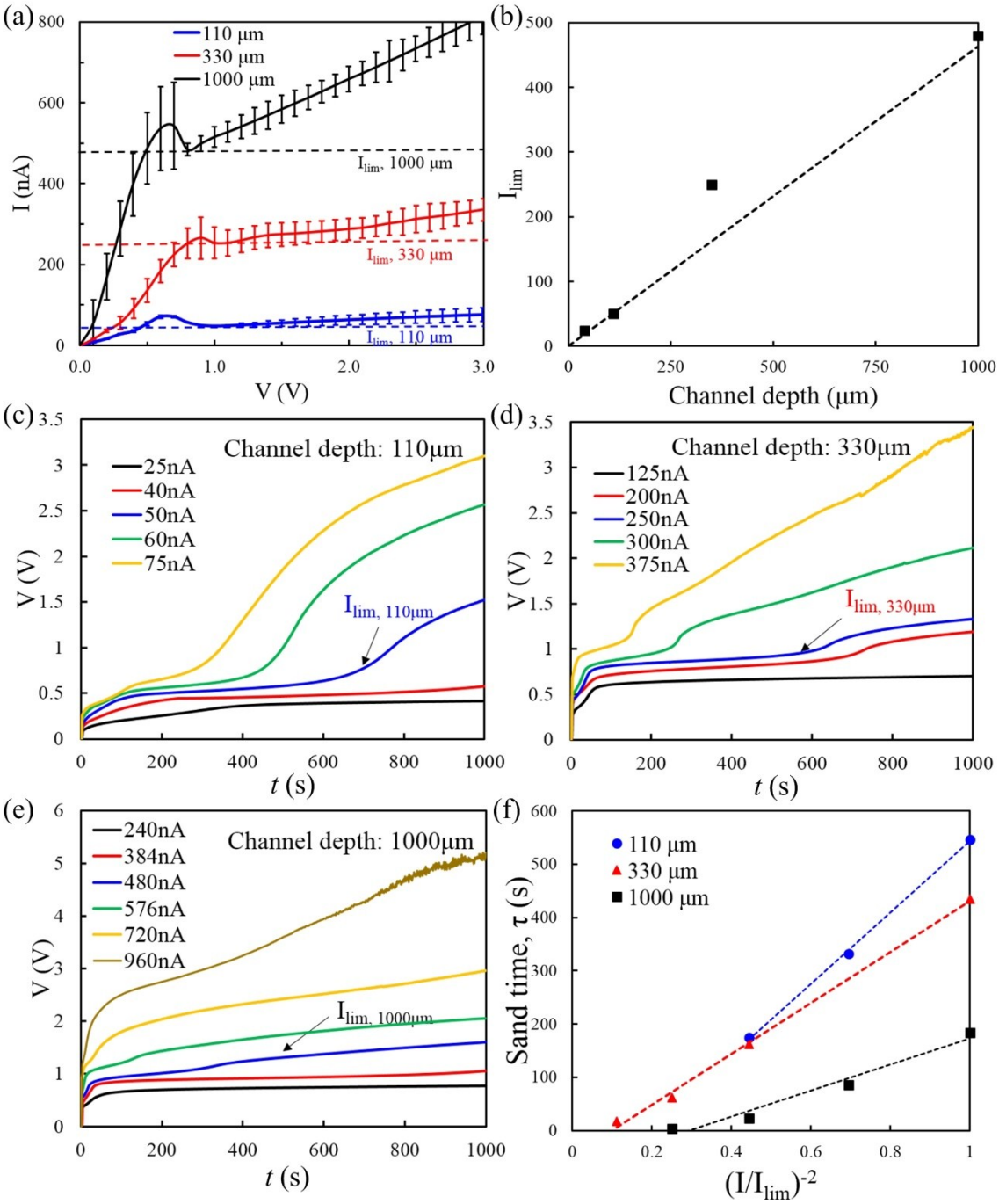

Supplementary Figure 3: Characterization of the CP effect within the membrane-microchannel system without ET flow and for various microchannel depths. (a) Current-voltage (*I-V*) response with a voltage sweep rate of 1mV/s, where the limiting currents, I_{lim}, are indicated by dashed lines. (b) Correlation between I_{lim} and channel depth. The dashed line shows a linear fit extracted from $I_{\text{lim}} = 2\text{zFDc}_0(2dW)/L$, where *d*, *W* and *L* are channel depth, width and length, respectively. (c, d, e)

Chronopotentiometric (V-t) response with various currents (0.5, 0.8, 1, 1.2, and 1.5 × I_{lim}) for various microchannel depths. (f) Sand time vs. the inverse of the current density squared.

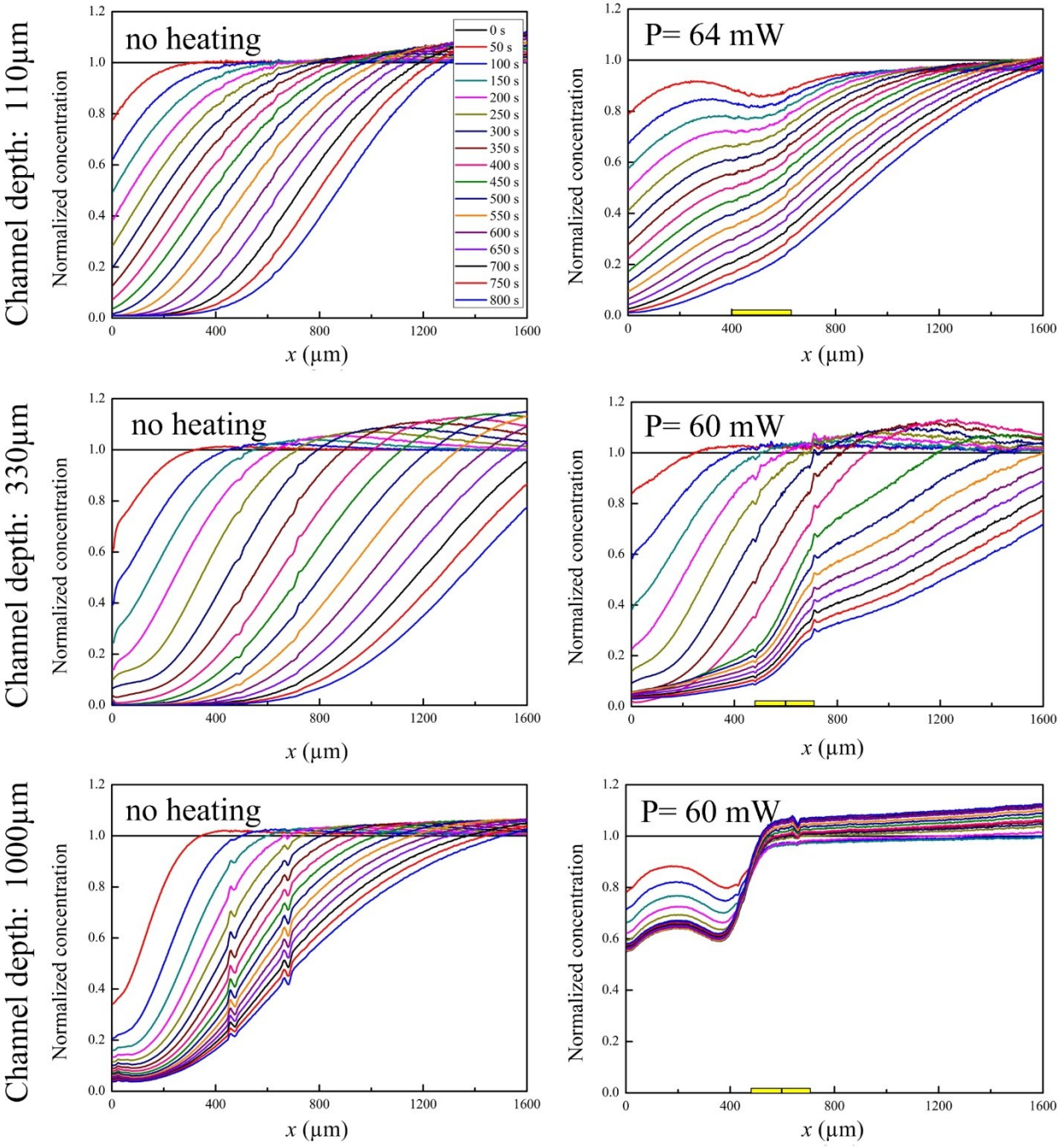

Supplementary Figure 4: Time evolution of depletion layer growth (intensity normalized by its bulk value) at the anodic side of the microchannel-membrane interface of the systems relating to Fig. 3(c, f, i).

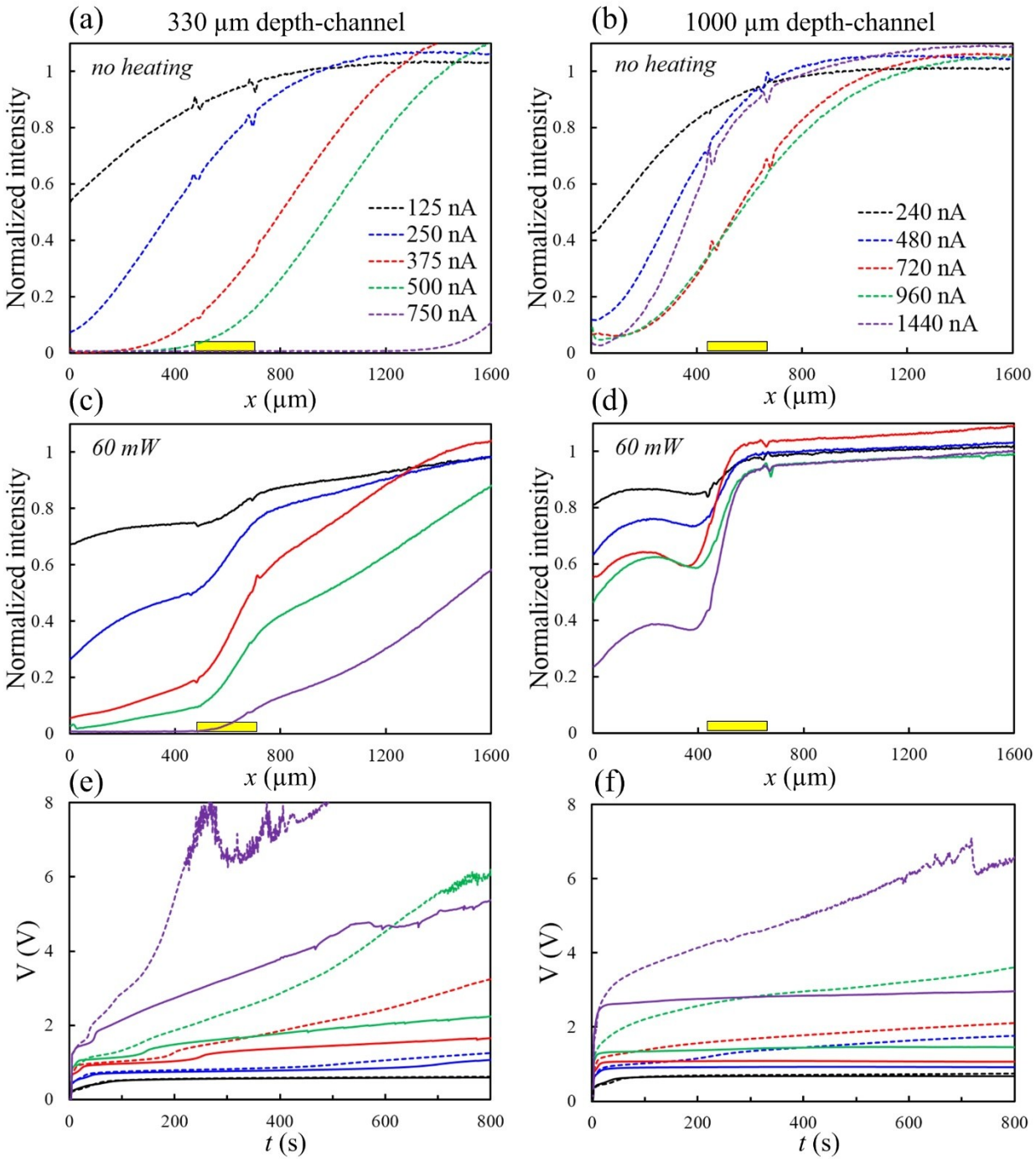

Supplementary Figure 5: The effect of ET-induced flow on CP behavior for various applied external currents (0.5, 1, 1,5, 2, and 3 × I_{lim}) in membrane-microchannel systems with 330 µm- (a, c, e) and 1000 µm-depth (b, d, e). The dashed and solid lines in all graphs represent the case of no-heating and applied

heating power of 60mW, respectively. (a-d) The normalized (by the bulk value) fluorescence intensities of depletion layer growth at $t = 500$s . (e, f) The corresponding V-t response.

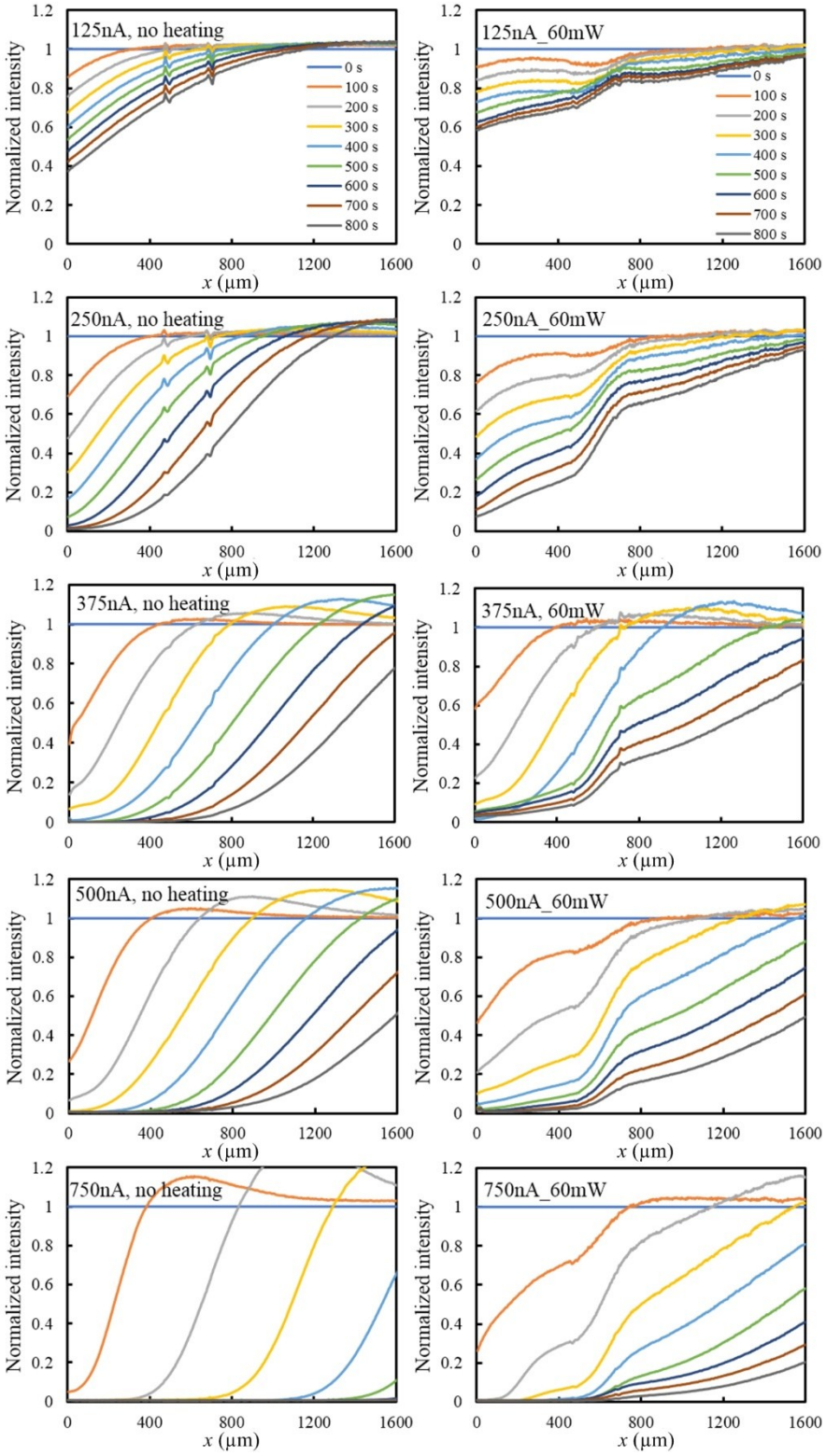

Supplementary Figure 6: Time evolution of depletion layer growth (intensity normalized by its bulk value) at the anodic side of the microchannel-membrane interface of the systems (channel depth 330 μm) as a function of various applied currents with/without heating.

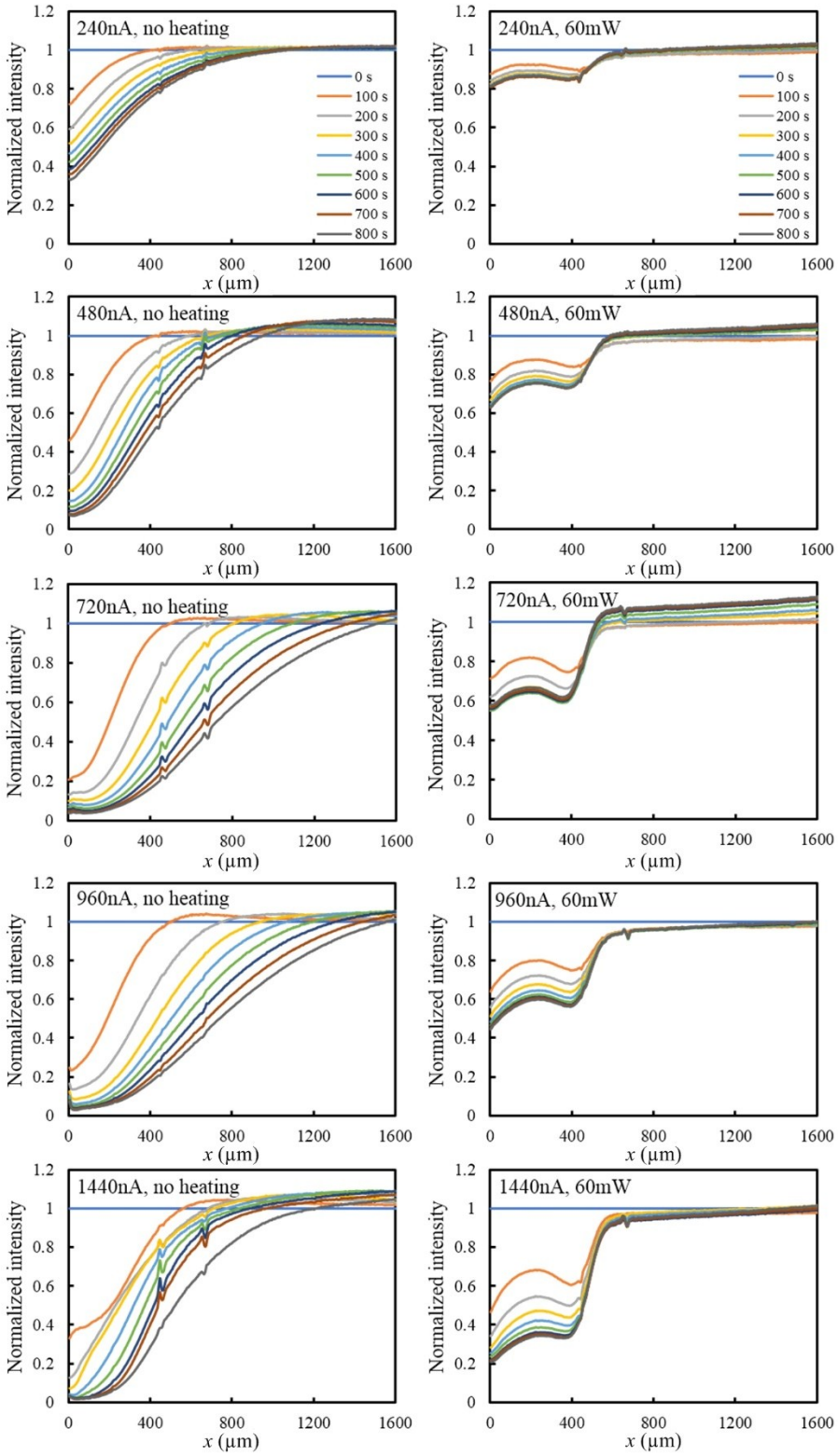

Supplementary Figure 7: Time evolution of depletion layer growth (intensity normalized by its bulk value) at the anodic side of the microchannel-membrane interface of the systems (channel depth 1000 μm) as a function of various applied currents with/without heating.

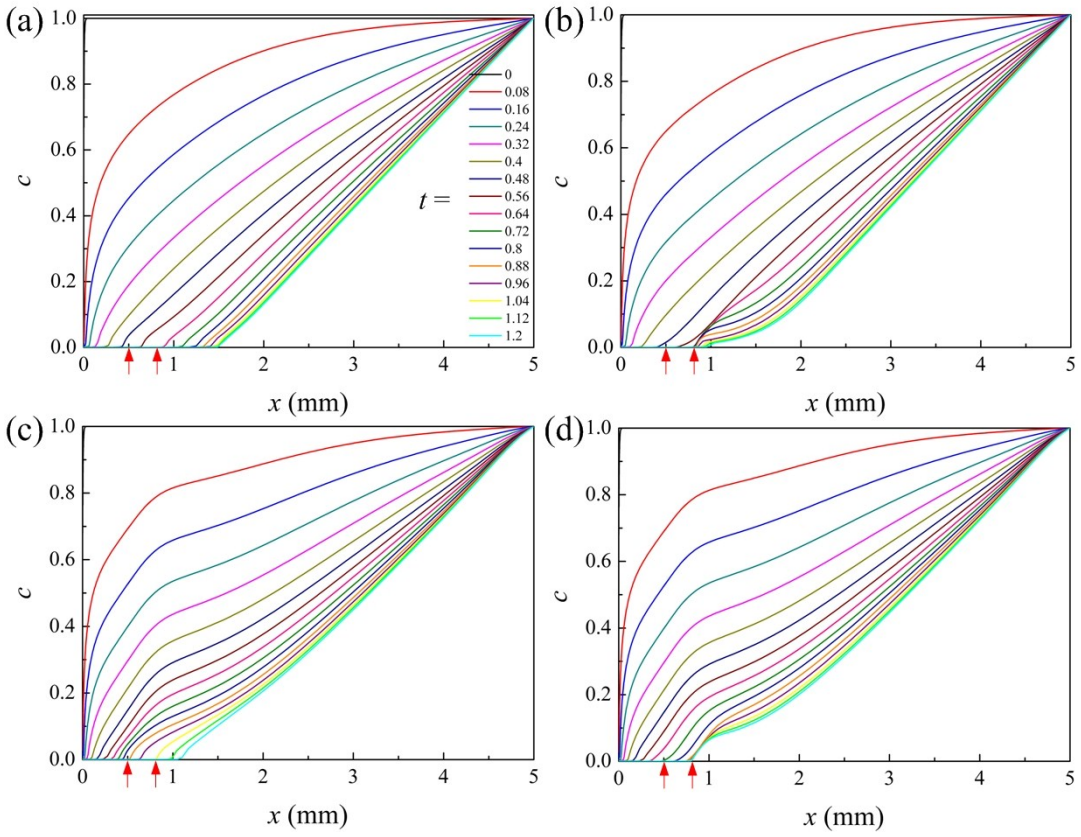

Supplementary Figure 8: Time evolution of the depletion layer in terms of its salt concentration distribution, $c=(c_+ + c_-)/2c_0$ for the cases of: a) no heating; (b) ET only; (c) NC only; (d) combined ET and NC. The applied current density is i = 1.45 $i_{\text{lim, 1D}}$ (where $i_{\text{lim,1D}}$ stands for the limiting current density in the 1D case). In all cases, EOF was accounted for by using a zeta potential of $\zeta = -10\,\text{mV}$. For the parameters of diffusion coefficient of ion pairs, viscosity, permittivity and thermal conductivity of fluid, the temperature-dependent physical properties were considered. The time, t, is normalized by the diffusion time, $t_d = L^2 / D$. A microchannel depth of 750μm was used in the simulations.

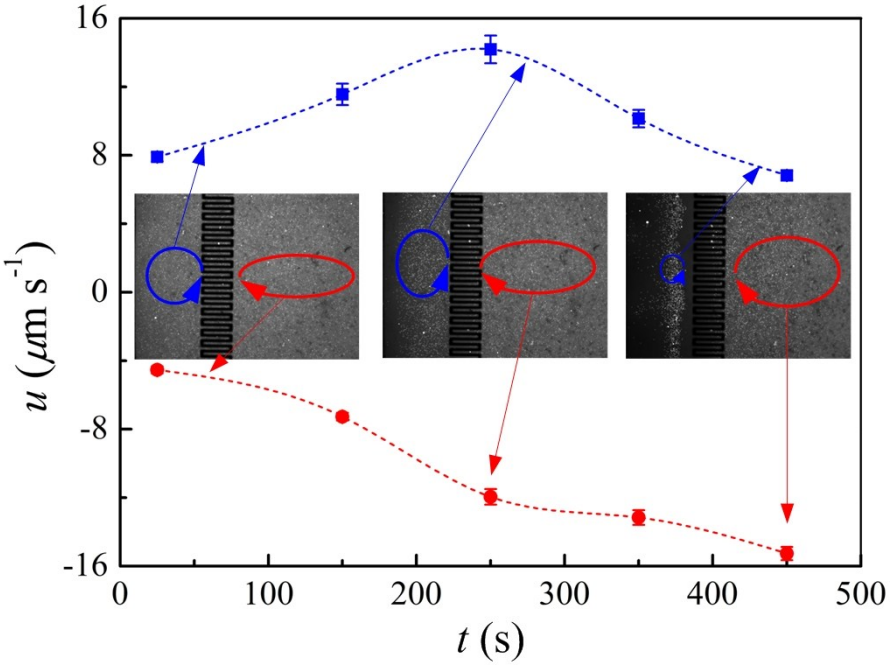

Supplementary Figure 9: The measured temporal change of the velocity component, *u,* within a membrane-microchannel system (d = 330 μm, z_1 = 100 μm) under the application of the heater (60 mW) and constant applied current (375 nA). The blue and red lines correspond to the velocities at the left and right sides of the heater, with measuring ranges 50 to 200 μm from the outer edges of the heater. The insets are microscopic images at time of 100, 300, and 500 s respectively, indicating the simultaneous occurrence and growth of the concentration-polarization layer.

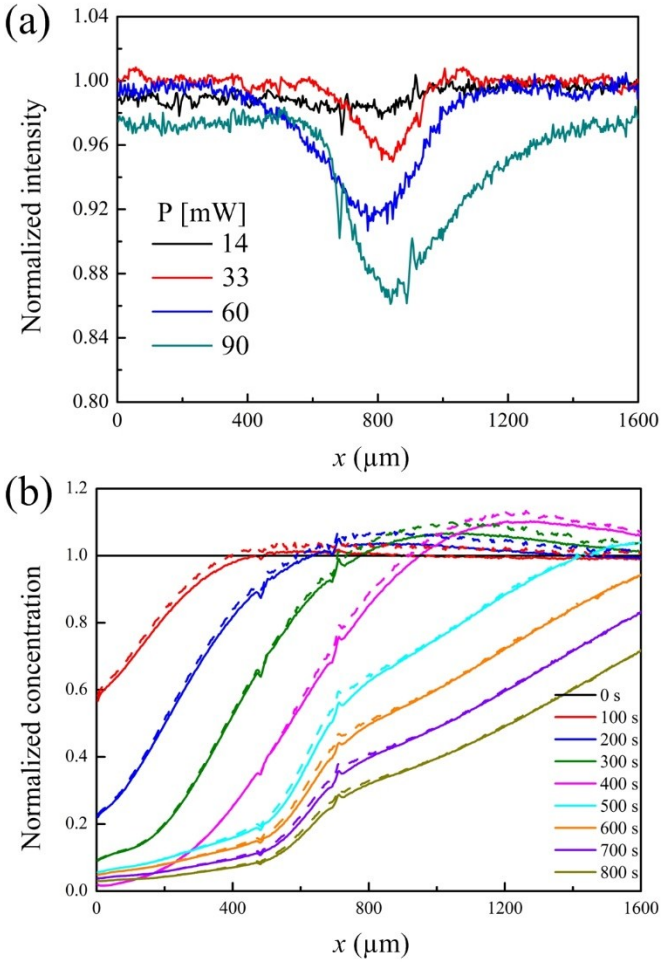

Supplementary Figure 10: Temperature effect on the intensity of the Dylight solution. (a) The measured normalized intensity along the x-axis, at 500s, within a membrane-less microchannel (d = 330 μm, z_1 = 100 μm), as a function of various applied heater power. (b) Comparison of the concentration intensity profiles in membrane-microchannel systems with 330 μm-depth (375nA, 60mW with heating power) with/without compensation by temperature dependency on Dylight solution. Dashed and solid lines indicate the compensated and un-compensated intensity profiles, respectively.